# Contrast-enhanced ultrasound imaging in vivo with laser-activated nanodroplets:

Heechul Yoon, *Georgia Institute of Technology*
Steven K. Yarmoska, *Emory University*
Alexander S. Hannah, *Emory University*
Changhan Yoon, *Inje University*
Kristina A. Hallam, *Emory University*
Stanislav Emelianov, *Emory University*

**Journal Title:** Medical Physics
**Volume:** Volume 44, Number 7
**Publisher:** Wiley | 2017-07-01, Pages 3444-3449
**Type of Work:** Article | Post-print: After Peer Review
**Publisher DOI:** 10.1002/mp.12269
**Permanent URL:** https://pid.emory.edu/ark:/25593/t0n0s

Final published version: http://dx.doi.org/10.1002/mp.12269

HHS Public Access

Author manuscript

*Med Phys*. Author manuscript; available in PMC 2018 July 01.

Published in final edited form as:

*Med Phys*. 2017 July ; 44(7): 3444–3449. doi:10.1002/mp.12269.

# Contrast-enhanced ultrasound imaging *in vivo* with laser-activated nanodroplets

**Heechul Yoon**[1], **Steven K. Yarmoska**[2], **Alexander S. Hannah**[2], **Changhan Yoon**[3], **Kristina A. Hallam**[2], and **Stanislav Y. Emelianov**[1,2,*]

[1]School of Electrical and Computer Engineering, Georgia Institute of Technology, Atlanta, Georgia 30332, USA

[2]The Wallace H. Coulter Department of Biomedical Engineering, Georgia Institute of Technology and Emory University School of Medicine, Atlanta, Georgia 30332, USA

[3]Department of Biomedical Engineering, Inje University, Gimhae, Gyeongnam 621-749, Korea

## Abstract

**Purpose—**This study introduces a real-time contrast-enhanced ultrasound imaging method with recently developed laser-activated nanodroplets (LANDs), a new class of phase-change nanometer-scale contrast agents that provides perceptible, sustained high-contrast with ultrasound.

**Methods—**In response to pulsed laser irradiation, the LANDs—, which contain liquid perfluorohexane and optical fuses—blink (vaporize and recondense). That is, they change their state from liquid nanodroplets to gas microbubbles, and then back to liquid nanodroplets. In their gaseous microbubble state, the LANDs provide high-contrast ultrasound, but the microbubbles formed *in situ* typically recondense in tens of milliseconds. As a result, LAND visualization by standard, real-time ultrasound is limited. However, the periodic optical triggering of LANDs allows us to observe corresponding transient, periodic changes in ultrasound contrast. This study formulates a probability function that measures how ultrasound temporal signals vary in periodicity. Then, the estimated probability is mapped onto a B-scan image to construct a LAND-localized, contrast-enhanced image. We verified our method through phantom and *in vivo* experiments using an ultrasound system (Vevo 2100, FUJIFILM VisualSonics, Inc., Toronto, ON, Canada) operating with a 40-MHz linear array and interfaced with a 10 Hz Nd:YAG laser (Phocus, Opotek Inc., Carlsbad, CA, USA) operating at the fundamental 1064 nm wavelength.

**Results—**From the phantom study, the results showed improvements in the contrast-to-noise ratio of our approach over conventional ultrasound ranging from 129% to 267%, with corresponding execution times of 0.10 s to 0.29 s, meaning that the developed method is computationally efficient while yielding high-contrast ultrasound. Furthermore, *in vivo* sentinel lymph node (SLN) imaging results demonstrated that our technique could accurately identify the SLN.

*Correspondence to: stas@gatech.edu.

**Disclosure of Conflicts of Interest**

The authors declare no competing financial interests.

**Conclusions—**The results indicate that our approach enables efficient and robust LAND localization in real time with substantially improved contrast, which is essential for the successful translation of this contrast agent platform to clinical settings.

### Keywords

Contrast-enhanced ultrasound; laser-activated nanodroplets; sentinel lymph node; perfluorocarbon nanodroplets; phase-change contrast agents; microbubbles

## 1. Introduction

Cancer is the second leading cause of death in the United States, and most cancer-related deaths are highly associated with metastasis.[1,2] Therefore, detecting and assessing the sentinel lymph node (SLN), which is the first lymph node to which cancer cells drain from a primary tumor, is crucial. To identify the SLN, researchers have explored numerous biomedical imaging techniques.[3–10] Classically, lymphoscintigraphy with radiocolloid injection has been widely used for preoperative lymph node imaging, but its imaging resolution is relatively low.[5] Magnetic resonance imaging (MRI) has shown promising results for nodal staging, but MRI is not cost effective and imaging lymph nodes during surgery and/or biopsies is challenging.[6] In addition, although positron emission tomography/computed tomography (PET/CT) has shown potential in preoperative scanning of lymph nodes, its sensitivity and specificity in identifying SLN is lower than those of lymphoscintigraphy or MRI.[11] Ultrasound is a cost-effective and non-invasive imaging modality that is able to guide SLN biopsies in real-time. Although ultrasound can be used to identify lymph nodes, the contrast between lymph nodes and the surrounding background is limited, and ultrasound alone cannot visualize which node receives drainage from the tumor. Accordingly, microbubbles have been used to improve contrast, but their relatively large size (a few microns) impedes their influx into the lymph node.[12,13] In addition, their circulation time is relatively short (a few minutes), limiting the duration of imaging sessions.[14]

To address these limitations of microbubbles, phase-changing nanodroplets that can be activated either acoustically or optically have been intensively investigated.[15–20] Because they remain in a stable liquid state until they are triggered, nanodroplets can circulate relatively longer and remain small enough to extravasate from tumor neovasculature. Once vaporized in response to an acoustic or optical trigger, nanodroplets become gaseous microbubbles, providing high-contrast ultrasound similar to conventional microbubbles. However, because nanodroplets usually consist of low-boiling-point materials (e.g., perfluoropentane (29°C) or perfluorobutane (−1°C)), they do not recondense back to the original liquid state after activation. More recently, our group and others have developed laser-activated nanodroplets (LANDs) containing liquid perfluorohexane and optical dye. LANDs repeatedly vaporize and recondense because the boiling point of perfluorohexane (56°C) is higher than physiological temperature (37°C).[21–23] This unique, repeatable phase-changing property of LANDs has enabled or improved many applications, including super-resolution imaging, background-free imaging, and photoacoustic imaging.[22,23] Fig. 1 shows the blinking dynamics of the LANDs. Before optical triggering, the LANDs remain liquid nanodroplets, producing very limited ultrasound echoes. However, once activated by pulsed

laser irradiation, the LANDs rapidly vaporize into gaseous microbubbles *in situ*, generating hyperechoic ultrasound signals until the LANDs completely recondense.[16,18,22,23] However, their gaseous period is relatively transient (several to hundreds of milliseconds), which limits human perception of LAND-based contrast.[22]

To overcome this limitation and to provide perceptible, sustainable LAND-based contrast in ultrasound, this work has developed an imaging method that effectively localizes the LANDs with high frame rate ultrasound imaging. In the method, we activate the LANDs periodically and capture the periodic blinking LANDs in ultrasound images, enabling the development of a fast, robust LAND-localization algorithm.

## 2. Materials and Methods

This study introduces a novel, contrast-enhanced imaging method that uses high frame rate ultrasound imaging to localize LANDs. This real-time imaging method is clinically applicable and provides superior contrast to conventional ultrasound. As illustrated in Fig. 2, our approach is based on LAND injection and optical activation, both of which are essential to the creation of contrast-enhanced LAND frames. Before injecting LANDs and initiating the laser, no localized LANDs are observable in contrast-enhanced frames. Without an optical trigger, localized LAND frames produce nearly imperceptible contrast because the LANDs have not vaporized and thus remain liquid droplets. However, once the pulsed laser irradiates local tissue containing LANDs, the vaporized particles become hyperechoic, allowing for construction of contrast-enhanced LAND images (yellow frames in Fig. 2). The recondensation process, however, is relatively fast; so to provide sustained contrast-enhanced imaging, this method uniquely exploits the periodic, repeated blinking in our LAND-localization algorithm. Overall, our imaging protocol reconstructs contrast-enhanced LAND image frames from the acquired ultrasound data at the rate of the pulse repetition frequency (PRF) of the laser. Fortunately, it does not require any sophisticated synchronization between the laser and the ultrasound systems, indicating that this approach is not limited in its utility. Until several laser pulses (usually, 3 to 5) activate the LANDs, it is only possible to build incomplete, transient LAND frames (blue). Yet after triggering several times, fully contrast-enhanced LAND frames (green) can be achieved.

The crux of the LAND localization method is that if a pixel in an image contains LANDs and the PRF of the laser pulses is constant, then we can induce repeated, periodic blinking of LANDs corresponding to this PRF. Thus, the temporal ultrasound signal for this pixel will contain regularly spaced peaks if the frame rate of ultrasound is also kept constant. The localization method assesses the consistency of the resultant peaks in ultrasound frames after tissue has been irradiated with multiple laser pulses. The PRF of the laser is defined as $M$ and the frame rate of ultrasound is defined as $R$. Thus, every $N$ frames ($N=R/M$) a single strong signal peak from the optically triggered LANDs is observed, as this corresponds to the ultrasound frame at which the LANDs are vaporized. Therefore, when irradiating with $L$ laser pulses, $L$ peaks occur. These $L$ peaks here are recorded in $L$ sets of $N$ ultrasound frames (i.e., $L{\cdot}N$ ultrasound frames contain $L$ peaks). The positions of these peaks can be any integer between 1 and $N$, as every set consists of $N$ frames and one of these $N$ frames

will include the corresponding peak. For every pixel of interest in the image, the set $S$, containing $L$ positions of peaks, is defined by

$$S=\{s_1, s_2, \ldots, s_L\} \quad (1)$$

where $s_1$, $s_2$, …, $s_L$ are positions of peaks created by $L$ number of laser pulses. Each peak is detected using a simple gradient operation. Then, a cost function with absolute differences of all two-combinations from $S$ is defined by

$$e(i)=|s_j - s_k|,\ i=1, 2, \ldots, \begin{pmatrix} L \\ 2 \end{pmatrix} \quad (2)$$

where $j$ and $k$ are 1, 2, …, $L$ and $j \neq k$. The cost function $e(i)$ in Eq. (2) contains differences between peak positions from all possible pairs of two. Only image pixels containing the LANDs can present periodically blinking periodic ultrasound, which results in small $e(i)$'s because these peaks are detected repeatedly and consistently. Therefore, this method counts the number of $e(i)$'s less than or equal to $d$, where $d$ is a threshold that determines the sensitivity of the algorithm, as $c(i)$ by

$$c(i)=\begin{cases} 1, & if\ e(i) \leq d \\ 0, & otherwise \end{cases},\ i=1, 2, \ldots, \begin{pmatrix} L \\ 2 \end{pmatrix} \quad (3)$$

Finally, this method formulates a probability function $P_{LAND}$ presenting the positional regularity of these peaks by

$$P_{LAND}=\frac{\sum_{i=1}^{\begin{pmatrix} L \\ 2 \end{pmatrix}} c(i)}{\begin{pmatrix} L \\ 2 \end{pmatrix}} \quad (4)$$

where the denominator is the number of all two-combinations of $L$ and the numerator is the number of two-combinations whose absolute difference is less than or equal to $d$. Thus, the probability function defined in Eq. (4) represents how regularly peaks occur in the pixel of interest. In summary, to localize the LANDs for each pixel, this method measures how mutually close the detected $L$ peaks are to temporal ultrasound sequences. The estimated probability in Eq. (4) is displayed on each pixel of a contrast-enhanced LAND frame, indicating the localizability of LANDs.

We synthesized the LANDs, consisting of an optical dye (Epolight 3072, Epolin, Inc., Newark, NJ, USA), liquid perfluorohexane (FluoroMed, L.P., Round Rock, TX, USA), an aqueous fluorosurfactant (Zonyl FSO, Sigma-Aldrich, St. Louis, MO, USA), and deionized

water, following detailed procedures from our previous work.[22] Briefly, we first dissolved 1 mg of dye in 250 μL of perfluorohexane solution and sonicated the solution for 30 s. Then, we mixed this solution and a mixture of 2.5 mL deionized water and 0.5 mL 1% v/v aqueous fluorosurfactant. We vortexed the solution for 10 s and sonicated it again for 5 minutes in a water bath. Finally, we washed the synthesized LANDs by centrifuging for 5 minutes at 1,000 relative centrifugal force (rcf) and resuspending in fresh deionized water. The diameter of the synthesized LANDs was 300 nm, as measured by a dynamic light scattering instrument (Zetasizer Nano ZS, Malvern Instruments, Malvern, Worcestershire, UK).

For our phantom and *in vivo* SLN imaging studies, we used a preclinical ultrasound system (Vevo 2100, FUJIFILM VisualSonics Inc., Toronto, ON, Canada) with a 40-MHz linear array transducer. The frame rate of ultrasound imaging was 288 Hz. To activate the LANDs, we used a 10-Hz Nd:YAG (neodymium-doped yttrium aluminium garnet) laser (Phocus, Opotek Inc., Carlsbad, CA, USA) at its fundamental 1064-nm wavelength, without synchronization with the ultrasound system. We acquired ultrasound images for approximately 2 s, and thus, several tens of laser pulses could be delivered per ultrasound acquisition. The measured optical fluence was 50 mJ/cm$^2$, far below the ANSI limit (100 mJ/cm$^2$) for safety.[24]

We fabricated a tissue-mimicking phantom containing a cylindrical LAND-labeled inclusion and a homogeneous background. The phantom consisted of 21 mL of 40% polyacrylamide (Thermo Fisher Scientific, Walthan, MA, USA), 850 μL of 10% aqueous ammonium persulfate (Sigma-Aldrich, St. Louis, MO, USA) solution, 106 μL of TEMED (Sigma-Aldrich, St. Louis, MO, USA), 0.2% w/w silica particles (U.S. Silica, Hurtsboro, AL, USA), 0.01% w/w graphite particles (Dixon Ticonderoga, Lake Mary, FL, USA), and 64 mL of deionized water. Detailed procedures can be found in [22]. Only the inclusion contained 0.1% v/v LANDs. Our *in vivo* study was performed under protocols approved by the Institutional Animal Care and Use Committee at The University of Texas at Austin. A BALB/c nu/nu mouse (Charles River Laboratories, Inc., Wilmington, MA, USA) was anesthetized and injected submucosally through the tongue with 40 μL of LANDs using a 30-gauge needle. Then, we allowed the LANDs to drain for 30 minutes and imaged the cervical lymph nodes in the mouse's neck. After imaging, we immediately euthanized the mouse.

We collected two-dimensional ultrasound IQ sequences and processed the data with custom-written codes using MATLAB (The MathWorks, Inc., Natick, MA, USA). When reconstructing LAND frames, we varied the value of $L$ (i.e., the number of sets of ultrasound sequences used) to investigate how the choice of $L$ affects the results. For the quantitative evaluation, we computed the contrast-to-noise ratio (CNR) values from B-scans alone and LAND-localized frames with two region-of-interests (inclusion and background) in the phantom as a function of $L$. We estimated 95% confidence intervals (CIs), where the number of replicates were 13, 11, 9, 7, and 5 with $L$ of 3, 5, 7, 9, and 11, respectively. In addition, to assess the practicality of the method, we evaluated the execution times in MATLAB by repeating processing with 100 trials to obtain average running times and their 95% CIs. The size of image was 1168 by 148 pixels.

## 3. Results and Discussion

The top plot in Fig. 3 shows a temporal profile of the linear ultrasound intensity measured on a pixel of the image containing LANDs. A corresponding movie is available online. The laser began pulsing at 0.4 s, and the pulse repetition interval of the laser was 0.1 s (i.e., 10 Hz). Thus, the repeated blinking behavior of LANDs was observable in the profile every 0.1 s from 0.4 s onward. In the figure, the algorithm allocated LAND frames (with $L$ = 3 and 5) and their corresponding ultrasound frames every 0.1s. When $L$ = 3, the image processing method was able to produce LAND frames at 0.3 s since it used three sets of ultrasound sequences to localize the LANDs. Equally, when $L$ = 5, this method could generate LAND frames as soon as five sets of ultrasound sequences were collected (i.e., the number of ultrasound frames containing five laser pulses). Then, it continued generating LAND frames every 0.1 s (i.e., every laser pulse). However, note that even if a LAND image was constructed at 0.3 s when $L$ was three, it yielded no contrast since the laser pulsing had not commenced. In addition, before three laser pulses were fired, LAND frames were incomplete, and so the two LAND frames at 0.4 s and 0.5s were incomplete, transient images. Finally, from 0.6 s onward, the algorithm was able to create fully contrast-enhanced LAND images. As a result, this method clearly localized the LAND-containing inclusion with $L$'s of both three and five. Table I summarizes the CNR values of both unprocessed B-scans and LAND frames and the averaged processing times of LAND localization with various $L$ (3 to 11). As $L$ increased, the CNR improvement increased, but increasing $L$ may also cause motion-induced errors. Hence, maintaining as small an $L$ as possible is desirable to avoid motion artifacts. The measured average processing times were all under 0.3 s per LAND frame without deliberate computational optimization. Depending on the choice of $L$, the frame rate of LAND-localized images ranged from 3 to 10 Hz, whereas the frame rate of B-scan was not compromised with this method (i.e., consistent at 288 Hz). These results indicate that our approach is practical and robust, and that it enables the real-time detection of LANDs necessary for future translational efforts.

In the *in vivo* study, we imaged the murine SLN with the same setup used in the *in vitro* study, and Fig. 4 shows the results. Again, a corresponding movie is available online. In Fig. 4, we overlaid B-scan ultrasound frames with LAND-localized frames ($L$ = 5). A temporal profile on a selected pixel in the lymph node containing LANDs shows their blinking dynamics in response to laser activation. As expected, the more laser pulses used to trigger the LANDs, the better the method can localize the LANDs, which correspond to the location of the SLN. After irradiating the tissue with 5 laser pulses, the SLN in Fig. 4 was identified at 0.7 s with improved contrast over ultrasound alone (i.e., unprocessed B-scans obtained from 0.1 s to 0.4 s in Fig. 4).

This study has demonstrated the potential of the developed LAND-localization method via phantom and *in vivo* results. However, the study has several limitations. First, we only showed the *in vivo* results obtained from a single mouse. Our continuing studies will include more animals to validate the method's robustness. In addition, for the clinical translation of this technique, not only should the ability to process the data in real time and provide high contrast be considered, but also the biocompatibility of LANDs should be examined. For example, the Epolight 3072 dye used in this study has not been FDA-approved, but our

previous work has shown that the FDA-approved indocyanine green (ICG) dye was successfully loaded in perfluorocarbon nanodroplets, indicating that the LAND platform has high translational potential.[18] Lastly, we have not explicitly investigated the stability of LANDs (i.e., the number of cycles of vaporization and recondensation that LANDs can endure in response to pulsed laser irradiation). In these experiments, LANDs were imaged for at least five minutes, which equals to 3,000 cycles with our 10 Hz laser, suggesting their ability to reliably vaporize and recondense. In addition, our previous work has demonstrated that the vaporization of the LANDs depends on selected laser energy, indicating that the LANDs activated below their vaporization threshold do not vaporize and remain in the liquid state.[18] Thus, to utilize the blinking ability of LANDs, a proper choice of laser energy is required and a laser fluence of 50 mJ/cm$^2$ in this study allowed the LANDs to vaporize and recondense repeatedly.

## 4. Conclusion

We have introduced a contrast-enhanced imaging method that relies on LANDs undergoing sustained and repeatable phase changes. The LANDs vaporize and recondense in response to pulsed laser irradiation; and given a constant laser PRF, they exhibit periodic peaks in the temporal ultrasound signal. Based on this unique blinking phenomenon, we have built an imaging method that determines how regularly the temporal ultrasound fluctuates to create a LAND-localized frame. Through our *in vitro* study, we quantified a substantial improvement in CNR over conventional ultrasound achieved with low computational complexity. Furthermore, we successfully identified a murine SLN, illustrating the viability of our technique in a small animal model. These results demonstrate that our approach effectively and efficiently localized LANDs in real time, which is necessary for future work to translate this contrast agent platform to the clinic.

## Supplementary Material

Refer to Web version on PubMed Central for supplementary material.

## Acknowledgments

This work is supported by the National Institutes of Health under grants CA149740 and CA158598 and by a grant from the Breast Cancer Research Foundation.

## References

1. Siegel RL, Miller KD, Jemal A. Cancer statistics, 2015. CA: A Cancer Journal for Clinicians. 2015; 65(1):5–29. DOI: 10.3322/caac.21254 [PubMed: 25559415]
2. Spano D, Heck C, De Antonellis P, Christofori G, Zollo M. Molecular networks that regulate cancer metastasis. Seminars in Cancer Biology. 2012; 22(3):234–249. DOI: 10.1016/j.semcancer.2012.03.006 [PubMed: 22484561]
3. Somasundaram SK, Chicken DW, Keshtgar MRS. Detection of the sentinel lymph node in breast cancer. British Medical Bulletin. 2007; 84(1):117–131. DOI: 10.1093/bmb/ldm032 [PubMed: 18174216]
4. Ahmed M, Purushotham AD, Douek M. Novel techniques for sentinel lymph node biopsy in breast cancer: A systematic review. The Lancet Oncology. 2014; 15(8):e351–e362. DOI: 10.1016/S1470-2045(13)70590-4 [PubMed: 24988938]

5. Moncayo VM, Aarsvold JN, Alazraki NP. Lymphoscintigraphy and sentinel nodes. Journal of Nuclear Medicine. 2015; 56(6):901–907. DOI: 10.2967/jnumed.114.141432 [PubMed: 25931478]
6. Kuijs VJL, Moossdorff M, Schipper RJ, Beets-Tan RGH, Heuts EM, Keymeulen KBMI, Smidt ML, Lobbes MBI. The role of mri in axillary lymph node imaging in breast cancer patients: A systematic review. Insights into Imaging. 2015; 6(2):203–215. DOI: 10.1007/s13244-015-0404-2 [PubMed: 25800994]
7. Luke GP, Emelianov SY. Label-free detection of lymph node metastases with us-guided functional photoacoustic imaging. Radiology. 2015; 277(2):435–442. DOI: 10.1148/radiol.2015141909 [PubMed: 25997030]
8. Luke GP, Myers JN, Emelianov SY, Sokolov KV. Sentinel lymph node biopsy revisited: Ultrasound-guided photoacoustic detection of micrometastases using molecularly targeted plasmonic nanosensors. Cancer Research. 2014; 74(19):5397–5408. DOI: 10.1158/0008-5472.can-14-0796 [PubMed: 25106426]
9. Garcia-Uribe A, Erpelding TN, Krumholz A, Ke H, Maslov K, Appleton C, Margenthaler JA, Wang LV. Dual-modality photoacoustic and ultrasound imaging system for noninvasive sentinel lymph node detection in patients with breast cancer. Scientific Reports. 2015; 5:15748.doi: 10.1038/srep15748 [PubMed: 26510774]
10. Tourasse C, Dénier JF, Awada A, Gratadour A-C, Nessah-Bousquet K, Gay J. Elastography in the assessment of sentinel lymph nodes prior to dissection. European Journal of Radiology. 2012; 81(11):3154–3159. DOI: 10.1016/j.ejrad.2012.04.031 [PubMed: 22656671]
11. Singh B, Ezziddin S, Palmedo H, Reinhardt M, Strunk H, Tüting T, Biersack H-J, Ahmadzadehfar H. Preoperative 18f-fdg-pet/ct imaging and sentinel node biopsy in the detection of regional lymph node metastases in malignant melanoma. Melanoma Research. 2008; 18(5):346–352. DOI: 10.1097/CMR.0b013e32830b363b [PubMed: 18781133]
12. Sever AR, Mills P, Jones SE, Cox K, Weeks J, Fish D, Jones PA. Preoperative sentinel node identification with ultrasound using microbubbles in patients with breast cancer. American Journal of Roentgenology. 2011; 196(2):251–256. DOI: 10.2214/AJR.10.4865 [PubMed: 21257873]
13. Swartz MA. The physiology of the lymphatic system. Advanced Drug Delivery Reviews. 2001; 50(1–2):3–20. DOI: 10.1016/S0169-409X(01)00150-8 [PubMed: 11489331]
14. Ferrara K, Pollard R, Borden M. Ultrasound microbubble contrast agents: Fundamentals and application to gene and drug delivery. Annual Review of Biomedical Engineering. 2007; 9(1):415–447. DOI: 10.1146/annurev.bioeng.8.061505.095852
15. Sheeran PS, Dayton PA. Phase-change contrast agents for imaging and therapy. Current Pharmaceutical Design. 2012; 18(15):2152–2165. DOI: 10.2174/138161212800099883 [PubMed: 22352770]
16. Wilson K, Homan K, Emelianov S. Biomedical photoacoustics beyond thermal expansion using triggered nanodroplet vaporization for contrast-enhanced imaging. Nature Communications. 2012; 3:618.doi: 10.1038/ncomms1627
17. Sheeran PS, Rojas JD, Puett C, Hjelmquist J, Arena CB, Dayton PA. Contrast-enhanced ultrasound imaging and in vivo circulatory kinetics with low-boiling-point nanoscale phase-change perfluorocarbon agents. Ultrasound in Medicine & Biology. 2015; 41(3):814–831. DOI: 10.1016/j.ultrasmedbio.2014.10.020 [PubMed: 25619781]
18. Hannah A, Luke G, Wilson K, Homan K, Emelianov S. Indocyanine green-loaded photoacoustic nanodroplets: Dual contrast nanoconstructs for enhanced photoacoustic and ultrasound imaging. ACS Nano. 2014; 8(1):250–259. DOI: 10.1021/nn403527r [PubMed: 24303934]
19. Strohm E, Rui M, Gorelikov I, Matsuura N, Kolios M. Vaporization of perfluorocarbon droplets using optical irradiation. Biomedical Optics Express. 2011; 2(6):1432–1442. DOI: 10.1364/BOE.2.001432 [PubMed: 21698007]
20. Rapoport N, Nam K-H, Gupta R, Gao Z, Mohan P, Payne A, Todd N, Liu X, Kim T, Shea J, Scaife C, Parker DL, Jeong E-K, Kennedy AM. Ultrasound-mediated tumor imaging and nanotherapy using drug loaded, block copolymer stabilized perfluorocarbon nanoemulsions. Journal of Controlled Release. 2011; 153(1):4–15. DOI: 10.1016/j.jconrel.2011.01.022 [PubMed: 21277919]

21. Asami, R., Kawabata, K. Repeatable vaporization of optically vaporizable perfluorocarbon droplets for photoacoustic contrast enhanced imaging. Paper presented at: IEEE International Ultrasonics Symposium; 7–10 October, 2012; Dresden, Germany.

22. Hannah AS, Luke GP, Emelianov SY. Blinking phase-change nanocapsules enable background-free ultrasound imaging. Theranostics. 2016; 6(11):1866–1876. DOI: 10.7150/thno.14961 [PubMed: 27570556]

23. Luke GP, Hannah AS, Emelianov SY. Super-resolution ultrasound imaging in vivo with transient laser-activated nanodroplets. Nano Letters. 2016; doi: 10.1021/acs.nanolett.6b00108

24. American National Standards Institute Inc. American National Standard for Safe Use of Lasers. 2007. https://www.lia.org/PDF/Z136_1_s.pdf Accessed December 12, 2016

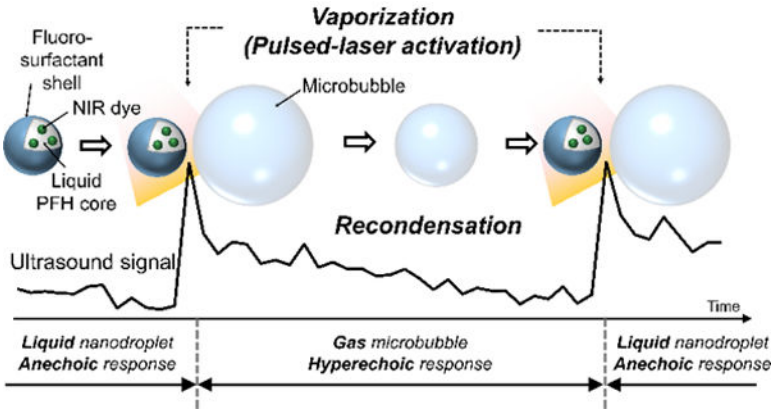


**FIG. 1.**

Vaporization and recondensation of laser-activated nanodroplets (LANDs) in response to an optical trigger. When activated, LANDs immediately produce strong ultrasound signals, which decrease as the LANDs recondense to native, liquid droplets.

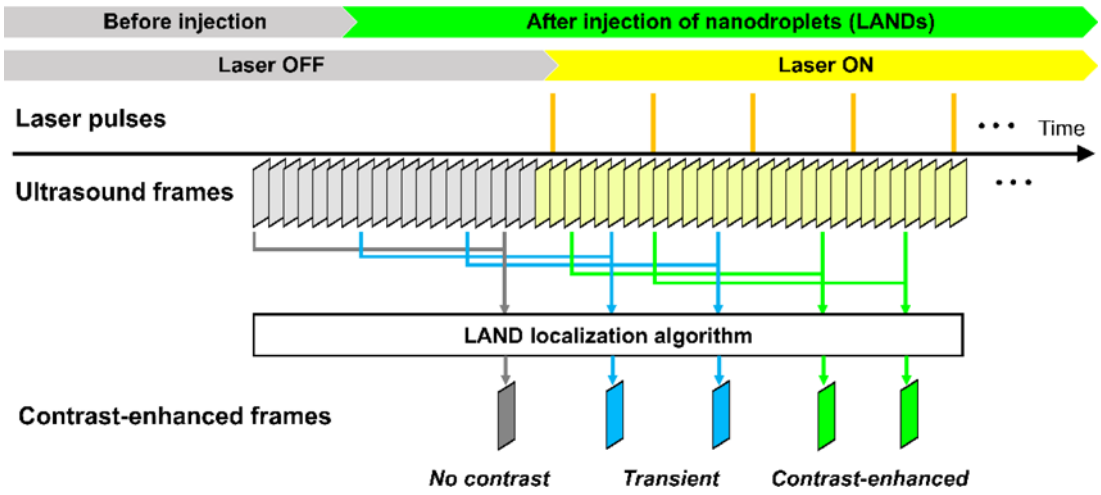


**FIG. 2.**

An imaging configuration for the localization of LANDs. After both injecting and triggering LANDs, this algorithm can reconstruct contrast-enhanced LAND image frames at the pulse repetition frequency of a laser system.

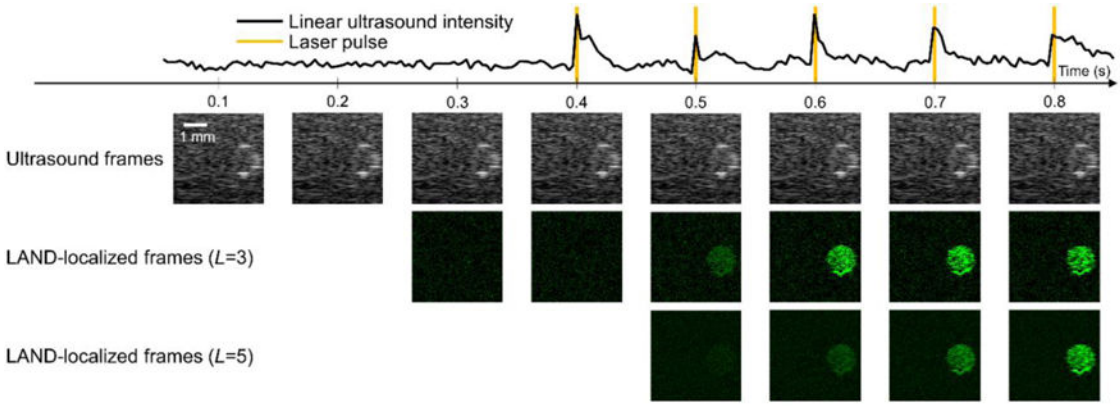


**FIG. 3.**

Ultrasound and LAND-localized images acquired in the phantom, containing a LAND-labeled inclusion as a function time. Laser pulses start activating the LANDs at 0.4 s. Corresponding two sets of the LAND-localized frames are shown using $L = 3$ and $L = 5$.

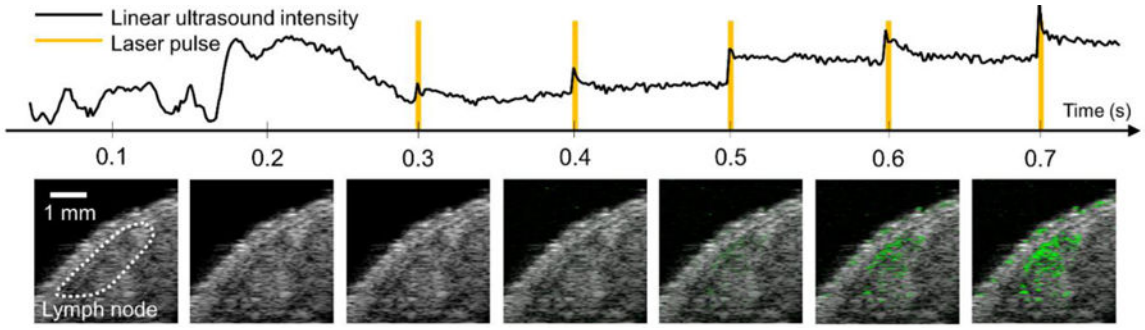


**FIG. 4.**

Ultrasound and LAND-localized images of *in vivo* murine SLN as a function of time. Laser pulses start activating the LANDs at 0.3 s. The LAND-localized frames with $L = 5$ are presented.

**TABLE I**

Quantitative assessment of LAND-localization results in a phantom

| Number of laser pulses (*L*) | Contrast-to-noise ratio | | | | Processing times | |
|---|---|---|---|---|---|---|
| | No. trials | B-scans | LAND frames | Mean improvement (%) | No. trials | Mean (95% CI) (ms) |
| 3 | 13 | 0.491 (0.478, 0.505) | 1.124 (1.089, 1.159) | 128.8 | 100 | 104.6 (104.0, 105.2) |
| 5 | 11 | 0.501 (0.491, 0.510) | 1.453 (1.436, 1.470) | 190.4 | | 135.7 (134.8, 136.6) |
| 7 | 9 | 0.507 (0.500, 0.514) | 1.637 (1.620, 1.655) | 223.2 | | 174.4 (173.7, 175.0) |
| 9 | 7 | 0.511 (0.505, 0.516) | 1.767 (1.752, 1.783) | 246.1 | | 227.4 (226.6, 228.1) |
| 11 | 5 | 0.513 (0.507, 0.518) | 1.888 (1.880, 1.896) | 267.3 | | 291.6 (291.0, 292.3) |